ACS APPLIED MATERIALS & INTERFACES

Research Article

www.acsami.org

Fe_2O_3/TiO_2 Tube-like Nanostructures: Synthesis, Structural Transformation and the Enhanced Sensing Properties

Chun-Ling Zhu,[†] Hai-Long Yu,[‡] Yue Zhang,[‡] Tie-Shi Wang,[‡] Qiu-Yun Ouyang,[‡] Li-Hong Qi,[‡] Yu-Jin Chen,[*,‡] and Xin-Yu Xue[*,#]

[†]College of Material Science and Chemical Engineering, Harbin Engineering University, Harbin 150001, China

[‡]College of Science, Harbin Engineering University, Harbin 150001, China

[#]College of Sciences, Northeastern University

Supporting Information

ABSTRACT: The paper describes for the first time the successful synthesis of Fe_2O_3/TiO_2 tube-like nanostructures, in which TiO_2 shell is of quasi-single crystalline characteristic and its thickness can be controlled through adjusting the added amount of aqueous $Ti(SO_4)_2$ solution. The characterization of samples obtained at different stages using transmission electron microscope indicates that the outer TiO_2 shell is changed gradually from amorphous and polycrystalline phase into quasi-single crystal under thermal actions through the Ostwald ripening process, accompanying the corrosion of the central parts of Fe_2O_3 nanorods, and the formation of small particles separating each other, leading to the special core/shell nanorods. Furthermore, Fe_2O_3/TiO_2 tube-like nanostructures can be transformed into Fe_2TiO_5 nanostructures after they are thermally treated at higher temperatures. Those nanostructures exhibit enhanced ethanol sensing properties with respect to the monocomponent. Our results imply that not only hollow nanostructures, but also a novel type of nanostructures can be fabricated by the present method for nanodevices.

KEYWORDS: *iron oxide, titanium dioxide, iron titanium oxide, gas sensing, hollow nanostructures, heterostructures*

1. INTRODUCTION

Core/shell and hollow nanostructures have attracted much interest in recent research because of their applications in catalysis, targeted drug delivery and photonic crystals, etc.[1−16] Recently, Liu et al. reported enhanced optical absorption of carbon nanotube (CNT)/CdS core−shell structures in the UV−visible region.[7] Zhu et al. synthesized CNT/ZnO nanocomposites and fabricated ultrafast nonlinear optical switch based on the hybrid system.[8] Kuang et al. observed the new luminescence properties from ZnO/SnO_2 core−shell nanostructures induced by the epitaxial interfaces.[9] Kim et al. prepared SnO_2/InO_3 core−shell nanowires which could be used as Li ion battery electrodes.[10] Very recently, Zhu et al. synthesized carbon-strabilized iron nanoparticles for environmental remediation,[11] and Zhang et al. fabricated Fe-sillica nanoparticle/polyurethane composites as electromagnetic field shielding materials.[12] Therefore, so far, various preparation strategies have been developed to fabricate hollow or core/shell nanostructures, including the Kirkendall effect,[17] acid etching,[18] corrosion-aided Ostwald ripening,[19] preferential dissolution,[20,21] sonichemical process,[22,23] and etc.

TiO_2 and Fe_2O_3, as two kinds of important semiconductors, have increasingly gained attention over the past decade.[22−38] Recently, nanohybrids based on these two materials have been synthesized in order to extend their applications. For example, TiO_2 nanotubes coated with ultralsmall superparamagnetic iron oxide can be detected by magnetic resonance imaging and have promising applications in the therapeutics;[29] Fe-doped TiO_2 can be used as chemical catalysts;[30−33] Fe_2O_3/TiO_2 mixtures act as the building-blocks for a high performance dye-sensitized solar cell;[34] α-Fe_2O_3/TiO_2 solid solutions and γ-Fe_2O_3/TiO_2 thick films can be used as gas sensing materials for detecting ethanol vapor;[35,36] α-Fe_2O_3-filled TiO_2 nanotubes or α-Fe_2O_3-covered TiO_2 surfaces show enhanced photoactivity by hematite-induced recombination versus surface-specific ractivity.[38] Therefore, the heteronanostructures based on Fe_2O_3 and TiO_2 have potential applications in many areas. However, to the best of our knowledge, there have been very few studies on synthesis and structural transformation of Fe_2O_3/TiO_2 tubular-like nanostructures for ethanol gas sensors.

Here we report for the first time the successful synthesis of 1 D Fe_2O_3/TiO_2 tube-like nanostructures with quasi-single crystalline TiO_2 shells through a controllable way. The special core/shell nanostructures exhibit enhanced ethanol sensing properties with respect to the monocomponent, with the heterojunction barrier-controlled sensing mechanism proposed. Furthermore, Fe_2TiO_5 nanostructures with different morphologies can be also obtained after further thermal treatments of 1 D Fe_2O_3/TiO_2 tube-like nanostructures. Our results imply that not only hollow nanostructures, but also a novel type of nanostructures, with interesting applications in nanodevices, can be synthesized by such proposed method.

2. EXPERIMENTAL DETAILS

2.1. Synthesis of 1 D Fe_2O_3/TiO_2 tube-like nanostructures. All of the chemicals were of analytical grade and were used as received. First, α-Fe_2O_3 nanorods were obtained using the modified method reported by Jia and his co-workers.[20,21] Simply, specific amount of

Received: September 15, 2011
Accepted: January 20, 2012
Published: January 20, 2012

dx.doi.org/10.1021/am201689x | ACS Appl. Mater. Interfaces 2012, 4, 665−671

$FeCl_3$, and $NH_4H_2PO_4$ were added into 40 mL of water under vigorous stirring; the concentrations of $FeCl_3$, and $NH_4H_2PO_4$ in the final mixture were 0.02 and 7.15×10^{-4} mol/L, respectively. The mixture was then transferred into a Teflon-lined stainless steel autoclave with a capacity of 50 mL for hydrothermal treatment at 220 °C for 4 h. As the autoclave cooled down to room temperature by it self, the precipitates were separated by centrifugation, washed with distilled water and absolute ethanol, dried in air.

0.075 g of the as-synthesized Fe_2O_3 nanorods were dispersed into 100 mL of distilled water under vigorously stirring. Then 50 mL of 0.0325 mol/L $Ti(SO_4)_2$ aqueous solution was added into the suspension in 1.5 h at 30 ± 2 °C.[39] The mixture was stirred for another 3 h at the same temperature, and then aged at the room temperature for 2 h. The precipitates were separated by centrifugation, washed with distilled water and absolute ethanol, dried in air. The sample obtain at this stage was treated at 360 °C for 6 h under a mixture of Ar/H_2 flow, and at 500 °C for 2 h and then 600 °C for another 2 h under the ambient atmosphere. Then, the sample was allowed to cool down to room temperature.

2.2. Synthesis of Fe_2TiO_5 nanostructures. Two kinds of Fe_2TiO_5 nanostructures with different morphologies were obtained after the 1 D Fe_2O_3/TiO_2 tube-like nanostructures were thermally treated at 800 °C for 2 h and 1000 °C for 2 h, respectively.

2.3. Sensor fabrication. The fabrication process of the sensors using these nanostructures was described elsewhere.[40,41] Briefly, the sensing materials were dispersed in ethanol, and a drop was spun on a ceramic tube between metal electrodes to form a thin film. A heating wire in the ceramic tube was used to control the working temperature of the sensor. The sensor response (S) to target gases is defined as $S = R_a/R_g$, where R_a is the sensor resistance in air, and R_g is the resistance in target−air mixed gas.

3. RESULTS AND DISCUSSION

3.1. Structrual characterization. *3.1.1. Structrual characterization of Fe_2O_3/TiO_2 tube-like nanostructures.* The overall crystallinity and purity of the as-synthesized samples were investigated by X-ray powder diffraction (XRD) and transmission electron microscope (TEM) measurement. As shown in Figure 1, the indexed diffraction peaks by "#" and "*" symbols in the XRD pattern confirm the presence of α-Fe_2O_3 (ICDD 33−0664) and TiO_2 (ICDD 12−1272) in the final product. Energy dispersive spectroscopy (EDS) spectrum reveals that the final product consists of Fe, O and Ti elements, and the atomic ratio of Fe to Ti is about 2.3:1, as shown in Figure S1. The above results indicate that the products obtained in the above are Fe_2O_3/TiO_2 nanostructures with high purity and crystalline quality.

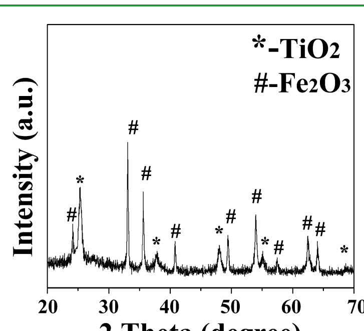

Figure 1. XRD pattern of 1 D Fe_2O_3/TiO_2 tube-like nanostructures.

Figure 2a displays the TEM image of the 1 D Fe_2O_3/TiO_2 nanostructures. On one hand, the central parts of the Fe_2O_3 nanorods have been disintegrated into small particles; whereas the outer TiO_2 wall is dense and smooth, leading to the formation of 1 D tube-like structures as overall morphology. The average diameter and length of the 1 D tube-like nanostructures and the thickness of the outer wall are 120, 400, and 23.5 nm, respectively. The HRTEM image (Figure 2b) reveals that the outer shell is quasi-single crystalline, in which the lattice spacing can be determined to be 0.348 nm, corresponding to the (101) plane of anatase TiO_2. Two spots presented in the Fourier transform image further confirm the quasi-single crystalline characters of the outer TiO_2 shell, as shown in the inset of Figure 2b.

Through the analyses of the products in the different synthesis stages, we suggest that the following mechanism is responsible for the formation of the tube-like core/shell nanostructures, as shown in the Scheme 1. Fe_2O_3/ amorphous TiO_2 (a-TiO_2) core/shell nanostructures were first obtained after the hydrolysis of $Ti(SO_4)_2$ in the solution containing Fe_2O_3 nanorods. The outer TiO_2 shell is very smooth and its thickness is about 21 nm, as shown in Figure 3a. The fact that only the diffraction peaks from Fe_2O_3 are observed in the XRD pattern (Figure 3b), indicates that the TiO_2 shell is amorphous at this stage. When the Fe_2O_3/TiO_2 core/shell nanostructures were exposed to hydrogen at 360 °C for 6 h, their structures changed significantly. The Fe_2O_3 and the amorphous TiO_2 were transformed into cubic Fe_3O_4 and anatase TiO_2, respectively (confirmed by XRD pattern, shown in Figure S2). TEM, HRTEM and selective-area electron diffraction (SAED) (Figure 3c and 3d) show that the surface of outer shell, which consisted of polycrystalline TiO_2 particles with an average diameter of 4 nm, is changed to be relatively roarse. Thus, Fe_3O_4/polycrystalline TiO_2 (p-TiO_2) core/shell nanorods were obtained at the stage. It is worth noting that micropores can be produced in the cores under the reducing treatment, which is helpful to the formation of Fe_2O_3/TiO_2 tube-like nanostructures in the subsequent treatments.[21,23] After the Fe_3O_4/TiO_2 core/shell nanostructures were thermally treated at 500 °C for 2 h under the ambient condition, the outer TiO_2 shell became dense and smooth, and its thickness decreased to about 17 nm, as shown in Figure 3e. HRTEM and the Fourier transform images (Figure 3f) indicate that the degree of crystallinity of the TiO_2 shell is improved. On the other hand, the Fe_3O_4 was transformed to Fe_2O_3, including α-Fe_2O_3 and γ-Fe_2O_3 phases (proved by XRD measurement, shown in Figure S3). Simultaneously, the outer layer of the Fe_2O_3 got thinner slightly because the high thermal energy was exposed to the core part. Finally the outer TiO_2 shell was changed gradually from polycrystalline phase into quasi-single (qs) crystal under thermal treatment through the Ostwald ripening process companying with further corrosion of the center of Fe_2O_3 nanorods and the formation of small particles, separated by each other, leading to the special tube-like nanostructures with quasi-crystalline TiO_2 shell, as shown in Figure 2a and 2b. During this process, the outer Fe_2O_3 was diffused outward and formed an intimitate contact with the TiO_2 shell during the cooling process, leading to the increase of the thickness of the outer shell from 17 to 23.5 nm. It should be noted that the presence of the TiO_2 shell plays a very important role in the formation of the tube-like nanostructures because the 1 D structure of bare α-Fe_2O_3 nanorods still remained well through the same treated processes (see Figure S4). This also reveals that the TiO_2 shell make thermal energy to be more directly irradiated to the Fe_2O_3 core.

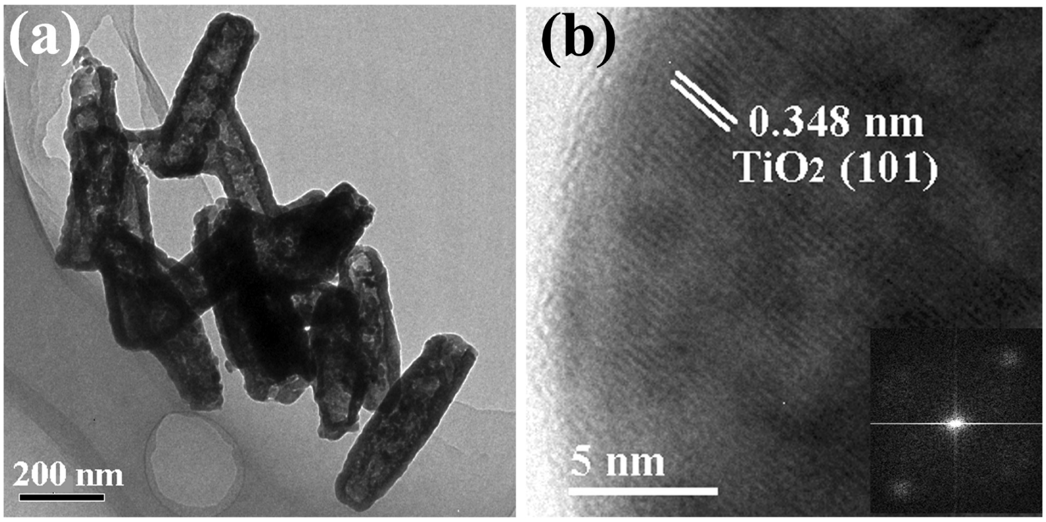

Figure 2. (a) TEM image, and (b) HRTEM and Fourier transform images of 1 D Fe_2O_3/TiO_2 tube-like nanostructures.

Scheme 1. Illustration of the growing processes of 1 D Fe_2O_3/TiO_2 tube-like nanostructures

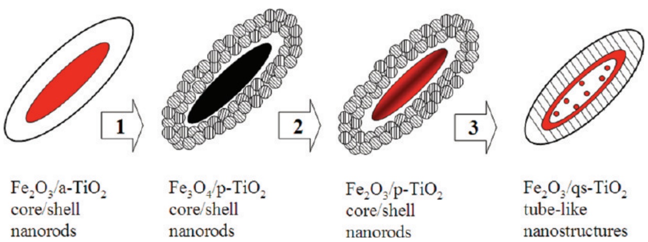

The XRD, SEM and TEM analyses above illustrate that the Fe_2O_3/TiO_2 tube-like nanostructures can be successfully prepared by the present method. Importantly, the thickness of outer wall can be tuned by simply varying the concentration of aqueous $Ti(SO_4)_2$ solution. Fe_2O_3/TiO_2 core/shell nanorods with armorphous shell of about 32 nm were fabricated as the concentration of $Ti(SO_4)_2$ solution was increased to 0.05 mol/L, as shown in Figure S5a. After the sample were exposed to hydrogen at 360 °C for 6 h and then thermally treated at 500 °C for 2 h under ambient conditions, the TiO_2 shell was very smooth and its thickness was about 28 nm, as shown in Figure S5b. Through the HRTEM and the Fourier transform images in Figure S5c, we can see that the outer TiO_2 shell is consisted of polycrystalline particles. After further treated at 600 °C for 2 h, the Fe_2O_3/TiO_2 tube-like nanostructures with the outer shell thickness of about 30 nm were fabricated, as shown Figure S5d. HRTEM and the Fourier transform images demonstrate that the outer TiO_2 is changed from polycrystalline phase to quasi-single crystal, as shown in Figure S5e. EDS spectrum (Figure S5f) shows the final product is consisted of Fe, Ti and O elements. Thus, through the proposed method, the thickness of the TiO_2 shell can be easily controlled.

3.1.2. Structrual characterization of Fe_2TiO_5 nanostructures. It is interesting that 1 D Fe_2O_3/TiO_2 tube-like nanostructures will transform into Fe_2TiO_5 nanostructures if they are further thermally treated at higher temperature under the ambient atmosphere. In Figure 4, the XRD patterns show the presence of Fe_2TiO_5 phase, after the sample being treated at 800 or 1000 °C for 2 h, repectively. All the diffraction peaks in the patterns can be indexed to orthorhombic Fe_2TiO_5 (ICDD 76−1158, lattice constants: a=3.739 Å, b=9.779 Å, and c=9.978 Å). Hollow Fe_2TiO_5 nanostructures with the length of ∼300 nm and the diameter of ∼180 nm were obtained after

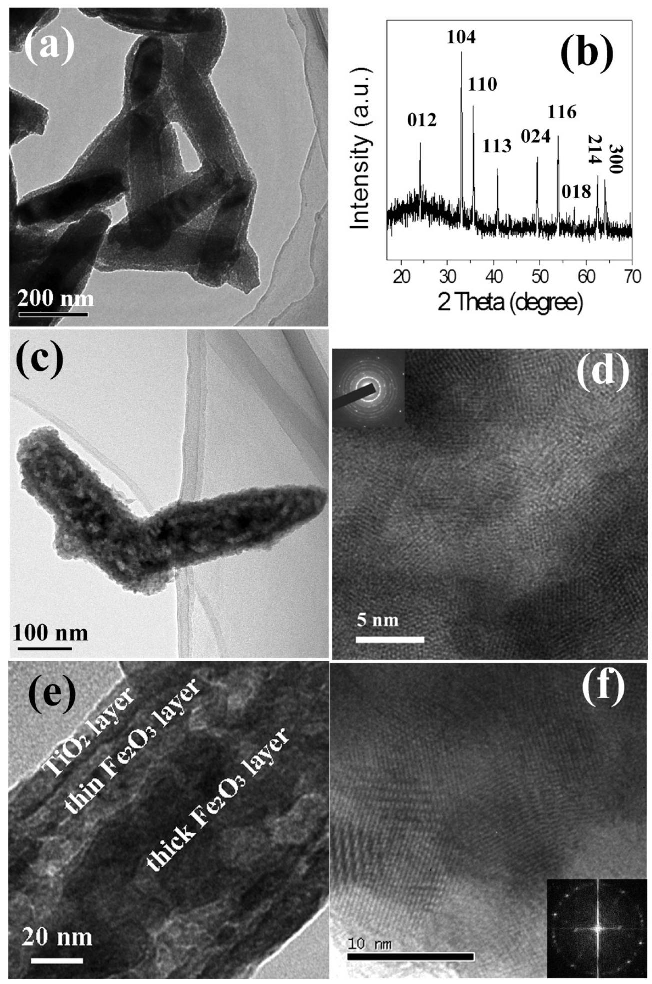

Figure 3. (a) TEM image and (b) XRD pattern of the Fe_2O_3/amorphous TiO_2 core/shell nanostructures. (c) T EM and (d) HRTEM images of Fe_3O_4/polycrystalline TiO_2 core/shell nanostructures; the inset in (d) is its SAED pattern. (e) TEM and (f) HRTEM images of the Fe_3O_4/polycrystalline TiO_2 core/shell nanostructures treated at 500 °C for 2 h under the ambient condition.

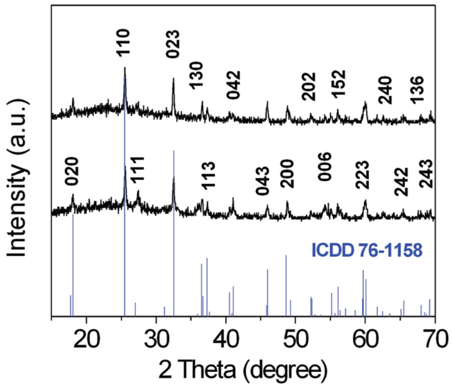

Figure 4. XRD patterns of Fe_2TiO_5 nanostructures obtained at (a) 800 °C and (b) 1000 °C.

the Fe_2O_3/TiO_2 tube-like nanostructures were treated at 800 °C for 2 h, as shown in Figure 5a. HRTEM and the Fourier transform images (Figure 5b) reveal that the sample is of quasi-single crystalline characteristics. The lattice spaces is 0.434 nm, corresponding to (021) plane of orthorhombic Fe_2TiO_5. If the Fe_2O_3/TiO_2 tube-like nanostructures were further treated at 1000 °C for 2 h, crystalline Fe_2TiO_5 particles with a diameter of 280 nm were fabricated, as shown in Figure 5c. HRTEM and the Fourier transform images (Figure 5d) demonstrate its quasi-single crystalline character. The lattice spaces is 0.50 nm, corresponding to (002) plane of orthorhombic Fe_2TiO_5. Thus, a new type of nanostructures is obtained by this very simple method, which may open a way for fabricating other new nanostructures.

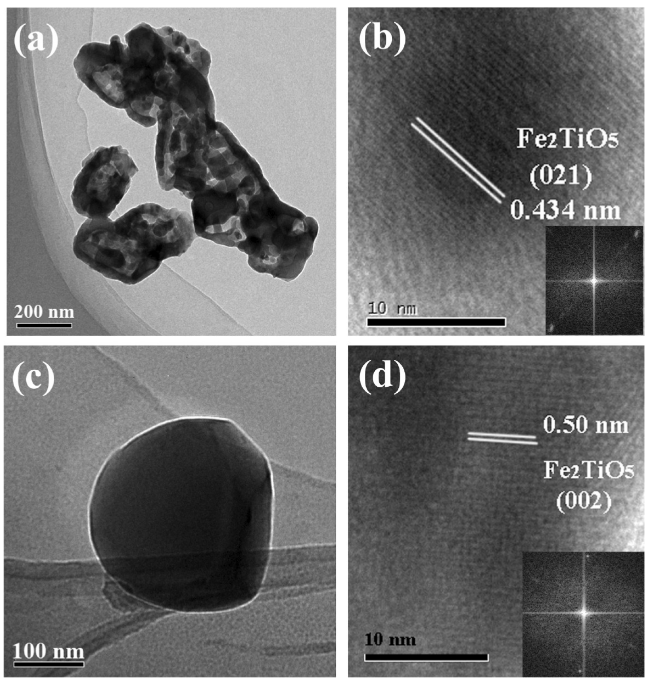

Figure 5. (a) TEM image and (b) HRTEM image of Fe_2TiO_5 nanostructures obtained at 800 °C, and the inset (b) shows the corresponding Fourier transform image, (c) TEM image and (d) HRTEM image of Fe_2TiO_5 nanostructures obtained at1000 °C for 2 h, and the inset (d) shows the corresponding Fourier transform image.

3.2. Gas sensing properties. *3.2.1. Gas sensing properties of Fe_2O_3/TiO_2 tube-like nanostructures.* Fe_2O_3 and TiO_2 are two kinds of important functional materials. Fe_2O_3 can be used as gas sensors and TiO_2 nanostructures have been widely investigated for photocatalysis. Recently, 1 D heteronanostructures have attracted much attention for chemical sensor because the sensitivity and selectivity can be manipulated by the component phases.[42,43] Thus the Fe_2O_3/TiO_2 tube-like nanostructures may have potential applications for gas sensors. For comparison, the bare Fe_2O_3 nanorods-based sensors were also prepared.

The bare Fe_2O_3 nanorods do not have any response to 500 ppm ethanol vapor until the working temperature is higher than 270 °C and the value of S is only about 1.5 at 300 °C. However, the Fe_2O_3/TiO_2 tube-like nanostructures have very significant response to ethanol vapor even at 180 °C, as shown in Figure 6a. The tube-like nanostructures have larger value of S at 320 °C, however, considering the stability of the sensors for practical application, we mainly investigated ethanol sensing properties at 270 °C. Figure 6b shows time-dependent response of the Fe_2O_3/TiO_2 tube-like nanostructures to ethanol vapor of different concentrations at 270 °C. It is found that the S value increases rapidly with the increase of ethanol concentration and it reaches 19.4 for 500 ppm ethanol, which is 1 order of magnitude higher than that of the bare Fe_2O_3 nanorods at 300 °C. Moreover, the tube-like nanostructures can test ethanol vapor at the ppb level. For example, the sensor response of the tube-like nanostructures to 500 ppb ehtanol reaches 1.9 at 270 °C, as shown in Figure 6b. These results show that the tube-like nanostructures exhibit enhanced ethanol sensing properties including stronger response, lower working temperature and trace detection, compared with the bare Fe_2O_3 nanorods. In addition, compared to other Fe_2O_3 -based composites, the tube-like nanostructures exhibited close or higher ethanol sensing properties. For example, the sensor response of Fe_2O_3–TiO_2 thick films to 150 ppm ethanol at 330 °C is about 2.0,[36] which is significantly lower than that of 1 D tube-like nanostructures fabricated in this work.

The mechanism of the enhanced sensor properties may be related to the synergetic effect from different gas sensing materials. In general, this effect requires that both of the sensing materials have strong response to the target gas.[43] In order to further clarify it, we prepared TiO_2 nanoparticles through the same processes as the preparation of the tube-like nanostructures, except that the Fe_2O_3 nanorods were not added.[44] The obtained TiO_2 nanoparticles had very weak response even when they were exposed to 1000 ppm ethanol at the tested temperature between 180 and 320 °C.[44] On the other hand, S is about 1.5 for the bare Fe_2O_3 nanorods to 500 ppm ethanol at 300 °C as discribed above. Those results imply that the bared Fe_2O_3 nanorods and TiO_2 nanoparticles both have weak response to ethanol. Therefore, the synergetic effect cannot explain the enhanced sensing properties very well. It is well-known that TiO_2 is a kind of effective catalyst, and it can help to photoelectrolyze water to produce H_2.[24] Therefore, the catalytic effect of TiO_2, like Au, Pt and Pd supported by metal oxides,[42] should be taken into consideration. But the TiO_2 shell in the tube-like nanostructures is relatively dense and thicker, thus the catalytic effect plays a relatively weak role in the enhanced gas sensing properties. Because the heterojunction formed at the interface between Fe_2O_3 and TiO_2, it should be the change of heterojunction barrier at the different gas atmospheres that contributes to the enhanced sensing properties. The band gap, work function and electron affinity of TiO_2 are 3.2, 4.2, and 3.9 eV, respectively,[44] which of Fe_2O_3 are 2.1, 5.6, and 4.71 eV, respectively.[45] Accordingly, the electron

dx.doi.org/10.1021/am201689x | ACS Appl. Mater. Interfaces 2012, 4, 665−671

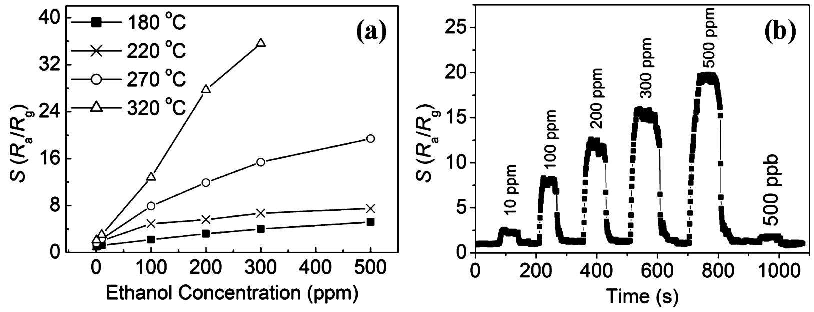

Figure 6. (a) Temperature-dependent sensor response of the Fe_2O_3/TiO_2 tube-like nanostructures to ethanol vapor and (b) Time-dependent response of the Fe_2O_3/TiO_2 tube-like nanostructures to ethanol vapor at 270 °C.

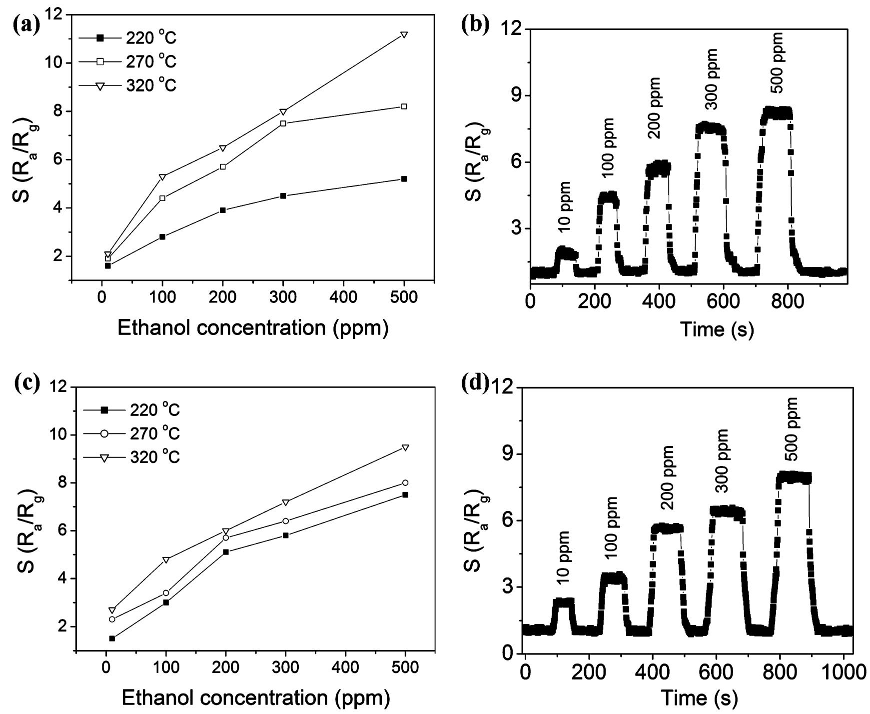

Figure 7. (a) Temperature-dependent sensor response of the Fe_2TiO_5 nanostructures obtained at 800 °C to ethanol vapor, (b) Time-dependent response of the nanostructures to ethanol vapor at 270 °C, (c) Temperature-dependent sensor response of the Fe_2TiO_5 nanostructures obtained at 1000 °C to ethanol vapor and (d) Time-dependent response of the nanostructures to ethanol vapor at 270 °C.

transfer occurs from the conduction band of TiO_2 to that of Fe_2O_3, leading to the formation of heterojunction barriers at their interfaces. As the tube-like nanostructures exposed to air, the barrier height ($q\Phi$) will increase because the electron in the TiO_2 bulk will be trapped when TiO_2 activate the dissociation of oxygen molecules into oxygen ions. According to the semiconductor theory, the resistance (R) related to heterojunction barrier can be expressed by, $R \propto B \exp(q\Phi/kT)$, where B is a constant related to ambient temperature, Φ heterojunction barrier, k the Boltzmann's constant and T the absolute temperature. Therefore, the conductivity of the nanostructures in air is very low (Figure S5). When the tube-like nanostructures are exposed to ethanol, the reaction between the adsorbed oxygen ions and the ethanol molecules will release electrons, which will flow into the conduction band of TiO_2 semiconductor, resulting in a decrease in the width and height of the barrier potential at the interfaces. In this case, the conductivity of the heterostructures will consequently be increased (Figure S5). Therefore, the tube-like nanostructures exhibit enhanced sensing properties to ethanol. Even if the barrier height only has a small change, the conductivity of the tube-like nanostructures change significantly. For example, assuming that the barrier change ($\Delta q\Phi$) is 0.14 eV, only about 1/10 of the work function difference between Fe_2O_3 and TiO_2, the maximum S value at 270 °C can be calculated as 19.6 (Figure S5). This reveals that the sensing mechanism can be used to explain the enhanced sensing properties.[45]

3.2.2. Gas sensing properties of Fe_2TiO_5 nanostructures. Iron titanium oxides have potential applications in the fields of magnetic semiconductors and optical fibers and catalysis.[46−50] Among these oxides, Fe_2TiO_5 is a kind of metal oxide semiconductors with band gap of about 2.3 eV. Its magnetic, optical and catalytic properties have attracted lot of attention. For example, Fe_2TiO_5 can be used as the anodes for photoelectrolysis of water.[46−50] However, to our knowledge, the sensing property of Fe_2TiO_5 nanostructures have been seldom investigated.[51,52]

Figure 7a shows the response of 800 °C-obtained Fe_2TiO_5 nanostructures to ethanol. It can be found that the values of the sensor response increas slowly with the increase of the working temperature. Figure 7b shows time-dependent response of the nanostructures to ethanol vapor of different concentrations at 270 °C. The *S* value slowly increases with the increase of ethanol concentration and it is 8.2 for 500 ppm ethanol. Fe_2TiO_5 nanostructures obtained at 1000 °C exhibited a similar sensing behavior to those obtained at 800 °C, but the sensor response is slightly lower, as shown in Figure 7c and 7d. For example, *S* is about 6.4 for 300 ppm ethanol, and 7.9 for 500 ppm ethanol at 270 °C, respectively. The ethanol sensing performances of Fe_2TiO_5 nanostructures are also significantly higher than that of the bare Fe_2O_3 nanorods, suggesting that they can be used as ethanol sensing materials. But the sensor responses of the nanostructures are weaker than those of 1 D Fe_2O_3/TiO_2 tube-like nanostructures, which may be attributed to the nonexistence of the heterojunctions in Fe_2TiO_5 nanostructures.

3.2.3. The selectivity of the sensors. Gas sensors for practical applications are required not only to have strong sensor response, but also very good selectivity to the targeted molecules. Therefore, the responses of the sensors based on 1 D Fe_2O_3/TiO_2 tube-like nanostructures and Fe_2TiO_5 nanostructures to 500 ppm H_2, NH_3, CH_4 and CO were also measured at 270 °C, as shown in the inset of Figure S6. The response values are all less than 1.5 for those gases, indicating that the sensors have very good selectivity to ethanol vapor. The selectivity of the metal oxide semiconductors to ethanol may be related to the following factors. First, it is related to the acidic-baisic properties of the oxide surfaces. Ethanol molecules will be converted into CO_2 and H_2O by the dehydrogenation process if the oxides exhibit basic characteristics:[53−55]

$$C_2H_5OH \rightarrow CH_3CHO + H_2 \quad (1)$$

$$CH_3CHO + 3O^- \rightarrow 2CO_2 + 2H_2O + 3e^- \quad (2)$$

Fe_2O_3 is known as a basic oxide while TiO_2 is an amphoteous oxide, which results in basic sites predminant in the surfaces of 1 D Fe_2O_3/TiO_2 tube-like nanostructures. Therefore, the tube-like nanostructures may favor ethanol's dehydrogenation into acetaldehyde. During this whole processes (eq 1 and eq 2), three electrons will be released from one ethanol molecule. But for other gases such as H_2 and CO, only one electron can be released under the same conditions. That is why the tube-like nanotubes exhibit a good selectivity to ethanol. However, it is worth noting that dynamics of the surface reaction plays an important role in the selectivity of the sensor. For example, oxides such as Fe_2O_3 and SnO_2 have very weak response to CH_4 except using Pd as a catalyt and at higher temperatures.[56,57]

Strong response and good selectivity of the sensors indicate their promising applications at the industrial level.

4. CONCLUSIONS

In summary, 1 D Fe_2O_3/TiO_2 tube-like nanostructures with quasi-single crystalline TiO_2 shell were successfully prepared by a controllable way. The presence of TiO_2 shell helps thermal energy to be more directly irradiated to the Fe_2O_3 core, which is helpful to the formation of the special core/shell nanorods. Fe_2TiO_5 nanostructures were also obtained after the thermal treatment of 1 D Fe_2O_3/TiO_2 tube-like nanostructures. The novel strategy developed here could be extended for the synthesis of other 1 D hollow nanocomposites. Furthermore, those nanostructures exhibited significantly enhanced ethanol sensing properties with respect to the monocomponent. Our results demonstrate that not only hollow nanostructures, but also a novel type of nanostructures can be fabricated by the present method for nanodevices.

■ ASSOCIATED CONTENT

Supporting Information

XRD patterns of the samples obtained at different stages, TEM image of bare Fe_2O_3 nanorods after the thermal treatment and 1 D Fe_2O_3/TiO_2 tube-like nanostructures with different shell thickness, Schematic diagram of heterojunction-controlled sensing mechanism, and the selectivity of the sensors. This information is available free of charge via the Internet at http://pubs.acs.org.

■ AUTHOR INFORMATION

Corresponding Author

*E-mail: chenyujin@hrbeu.edu.cn (Y.-J.C.); xuexinyu@mail.neu.edu.cn (X.-Y.X.).

Notes

The authors declare no competing financial interest.

■ ACKNOWLEDGMENTS

The authors acknowledge the support from the National Natural Science Foundation of China (Grant Nos. 51072038, 51102041 and 11000601), Program for New Century Excellent Talents in University (NECT-10-0049), and also Outstanding Youth Foundation of Heilongjiang Province (Grant No JC201008).

■ REFERENCES

(1) Cregan, R. F.; Mangan, B. J.; Knight, C.; Birks, T. A.; Russell, P. St. J.; Roberts, P. J.; Allan, D. C. *Science* **1999**, *285*, 1537−1539.
(2) Yin, Y.; Rious, R. M.; Erdonmez, C. K.; Hughes, S.; Somorjai, G. A.; Alivisatos, A. P. *Science* **2004**, *304*, 711−714.
(3) Kim, S. W.; Kim, M.; Lee, W. Y.; Hyeon, T. *J. Am. Chem. Soc.* **2002**, *124*, 7642−7643.
(4) Chen, Y. J.; Zhu, C. L.; Xue, X. Y.; Shi, X. L.; Cao, M. S. *Appl. Phys. Lett.* **2008**, *92*, 223101/1−223101/3.
(5) Fan, H. J.; Knez, M.; Scholz, R.; Nielsch, K.; Pippel, E.; Hesse, D.; Zacharias, M.; Gosele, U. *Nat. Mater.* **2006**, *5*, 627−631.
(6) Gao, J.; Zhang, B.; Zhang, X.; Xu, B. *Angew. Chem., Int. Ed.* **2006**, *45*, 1220−1223.
(7) Cao, J.; Sun, J. Z.; Hong, J.; Li, H. Y.; Chen, H. Z.; Wang, M. *Adv. Mater.* **2004**, *16*, 84−87.
(8) Zhu, Y. W.; Elim, H. I.; Foo, Y. L.; Yu, T.; Liu, Y. J.; Ji, W.; Lee, J. Y.; Shen, Z. X.; Wee, A. T.; Thong, J. T.; Sow, C. H. *Adv. Mater.* **2006**, *18*, 587−592.
(9) Kuang, Q.; Jiang, Z. Y.; Xie, Z. X.; Lin, S. C.; Lin, Z. W.; Xie, S. Y.; Huang, R. B.; Zheng, L. S. *J. Am. Chem. Soc.* **2005**, *127*, 11777−11784.
(10) Kim, D. W.; Hwang, I. S.; Kwon, S. J.; Kang, H. Y.; Park, K. S.; Choi, Y. J.; Choi, K. J.; Park, J. G. *Nano Lett.* **2007**, *7*, 3041−3045.
(11) Zhu, J. H.; Wei, S. Y.; Haldolaarachchige, N.; Young, D. P.; Guo, Z. H. *J. Phys. Chem. C* **2011**, *115*, 15304−15310.
(12) Zhang, D.; Wei, S. Y.; Kaila, C.; Su, X.; Wu, J.; Karki, A. B.; Young, D. P.; Guo, Z. H. *Nanoscale* **2010**, *2*, 917−919.
(13) Wei, S. Y.; Wang, Q.; Zhu, J. H.; Sun, L. Y.; Lin, H. F.; Guo, Z. H. *Nanoscale* **2011**, *3*, 4474−4502.
(14) Guo, Z. H.; Moldovan, M.; Young, D. P.; Henry, L. L.; Podlaha, E. J. *Electrochem. Solid-State Lett.* **2007**, *10*, E31−E35.
(15) Guo, Z. H.; Kumar, C. S. S. R.; Henry, L. L.; Doomes, E. E.; Hormes, J.; Podlaha, E. J. *J. Electrochem. Soc.* **2005**, *152*, D1−D5.
(16) Zhu, J. H.; Wei, S. Y.; Rutman, D.; Haldolaarachchige, N.; Young, D. P.; Guo, Z. H. *Ploymer* **2011**, *52*, 2947−2955.

(17) Gao, J.; Liang, G.; Cheung, J. S.; Pan, Y.; Kuang, Y.; Zhao, F.; Zhang, B.; Zhang, X.; Wu, E. X.; Xu, B. *J. Am. Chem. Soc.* **2008**, *130*, 11828−11833.
(18) Chen, Y. J.; Xue, X. Y.; Wang, T. H. *Nanotechnology* **2005**, *16*, 1978−1982.
(19) Wang, Z. X.; Wu, L. M.; Chen, M.; Zhou, S. X. *J. Am. Chem. Soc.* **2009**, *131*, 11276−11277.
(20) Jia, C. J.; Sun, L. D.; Luo, F.; et al. *J. Am. Chem. Soc.* **2008**, *130*, 16968−16977.
(21) Chen, Y. J.; Xiao, G.; Wang, T. S.; Ouyang, Q. Y.; Qi, L. H.; Ma, Y.; Gao, P.; Zhu, C. L.; Cao, M. S.; Jin, H. B. *J. Phys. Chem. C* **2011**, *115*, 13603−13608.
(22) Bang, J. H.; Suslick, K. S. *J. Am. Chem. Soc.* **2007**, *129*, 2242−2243.
(23) Zhu, C. L.; Zhang, M. L.; Qiao, Y. J.; Xiao, G.; Zhang, F.; Chen, Y. J. *J. Phys. Chem. C* **2010**, *114*, 16229−16235.
(24) Fujishima, A.; Honda, K. *Nature* **1972**, *238*, 37−38.
(25) O'Regan, B.; Grätzel, M. *Nature* **1991**, *353*, 737−740.
(26) Wu, Z. C.; Yu, K.; Zhang, S. D.; Xie, Y. *J. Phys. Chem. C* **2008**, *112*, 11307−11313.
(27) Liu, J. P.; Li, Y. Y.; Fan, H. J.; Zhu, Z. H.; Jiang, J.; Ding, R. M.; Hu, Y. Y.; Huang, X. T. *Chem. Mater.* **2010**, *22*, 212−217.
(28) Kartini, I.; Menzies, D.; Blake, d.; da Costa, J. C. D.; Meredith, P.; Riches, J. D.; Lu, G. Q. *J. Mater. Chem.* **2004**, *14*, 2917−2921.
(29) Papa, A. L.; Maurizi, L.; Vandroux, D.; Walker, P.; Millot, N. *J. Phys. Chem. C* **2011**, *115*, 19012−19017.
(30) Liu, F. D.; He, H. *J. Phys. Chem. C* **2010**, *114*, 16929−16936.
(31) Peng, B.; Meng, X. W.; Tang, F. D.; Ren, X. L.; Chen, D.; Ren, J. *J. Phys. Chem. C* **2009**, *113*, 20240−20248.
(32) Cai, L.; Liao, X. P.; Shi, B. *Ind. Eng. Chem. Res.* **2010**, *49*, 3194−3199.
(33) Yu, H. G.; Irie, H.; Shimodaira, Y.; Hosogi, Y.; Kuroda, Y.; Miyauchi, M.; Hashimoto, K. *J. Phys. Chem. C* **2010**, *114*, 16481−16487.
(34) Im, J. S.; Lee, S. K.; Lee, Y. S. *Appl. Surf. Sci.* **2011**, *257*, 2164−2169.
(35) Tan, O. K.; Cao, W.; Zhu, W.; Chai, J. W.; Pan, J. S. *Sens. Actuators, B* **2003**, *93*, 396−401.
(36) Reziescu, E.; Doroftei, C.; Reziescu, N.; Popa, P. D. *Phys. Status Solidi A* **2008**, *205*, 1790−1793.
(37) Kontos, A. I.; Likodimos, V.; Stergiopoulos, T.; Tsoukleris, D. S.; Falaras, P.; Rabias, I.; Papavassiliou, G.; Kim, D.; Kunze, J.; Schmuki, P. *Chem. Mater.* **2009**, *21*, 662−672.
(38) Jeon, T. H.; Choi, W. Y.; Park, H. W. *J. Phys. Chem. C* **2011**, *115*, 7134−7142.
(39) Xue, L.; Gao, W.; Zhang, D. Y.; Guo, X. F.; Ding, W. P.; Chen, Y. *J. Am. Chem. Soc.* **2006**, *128*, 11042−11043.
(40) Chen, Y. J.; Zhu, C. L.; Wang, L. J.; Gao, P.; Cao, M. S.; Shi, X. L. *Nanotechnology* **2009**, *20*, 045502/1−045502/6.
(41) Zhu, C. L.; Chen, Y. J.; Wang, R. X.; Wang, L. J.; Cao, M. S.; Shi, X. L. *Sens. Actuators, B* **2009**, *140*, 185−189.
(42) Kolmakov, A.; Klenov, D. O.; Lilach., Y; Stemmer, S.; Moskovits, M. *Nano Lett.* **2005**, *5*, 667−673.
(43) Chen, Y. J.; Zhu, C. L.; Shi, X. L.; Cao, M. S.; Jin, H. B. *Nanotechnology* **2008**, *19*, 205603/1−205603/5.
(44) Chen, Y. J.; Xiao, G.; Wang, T. S.; Zhang, F.; Ma, Y.; Gao, P.; Zhu, C. L.; Zhang, E. D.; Xu, Z.; Li, Q. H. *Sens. Actuators, B* **2011**, *156*, 867−874.
(45) Gratzel, M. *Nature* **2001**, *414*, 338−344.
(46) Liu, F. D.; He, H. *J. Phys. Chem. C* **2010**, *114*, 16929−16936.
(47) Liu, F.; He, H.; Zhang, C. *Chem. Commun.* **2008**, *44*, 2043−2045.
(48) Phani, A. R.; Ruggieri, F.; Passacantando, M.; Santucci, S. *Ceram. Int.* **2008**, *34*, 205−211.
(49) Ginley, D. S.; Bulter, M. A. *J. Appl. Phys.* **1977**, *48*, 2019−2021.
(50) Kozuka, H.; Kajimura, M. *J. Sol-Gel Sci. Technol.* **2010**, *63*, 155−162.
(51) Yu, R.; Li, Z.; Wang, D.; Lai, X.; Xing, C.; Yang, M.; Xing, X. *Scr. Mater* **2010**, *63*, 155−158.
(52) Bein, T.; Brown, K.; Fye, G. C.; Brinker, C. J. *J. Am. Ceram. Soc.* **1989**, *111*, 7640−7641.
(53) Idriss, H.; Seebauer, E. G. *J. Mol. Catal. A: Chem.* **2000**, *152*, 201−212.
(54) Fajardo, H. V.; Longo, E.; Probst, L. F. D.; Valentini, A.; Carreno, N. L. V.; Nunes, M. R.; Maciel, A. P.; Leite, E. R. *Nano. Res. Lett.* **2008**, *3*, 194−199.
(55) Shi, S. L.; Liu, Y. G.; Chen, Y. J.; Zhang, J. Y.; Wang, Y. G.; Wang, T. H. *Sens. Actuators, B* **2009**, *140*, 426−431.
(56) Kim, J. C.; Jun, H. K.; Huh, J. S.; Lee, D. D. *Sens. Actuators, B* **1997**, *45*, 271−277.
(57) Liu, F. M.; Zhang, Y. Q.; Yu, Y. S.; Xu, J.; Sun, J. B.; Lu, G. Y. *Sens. Actuators, B* **2011**, *160*, 1091−1097.